https://doi.org/10.5194/nhess-2024-113
Preprint. Discussion started: 24 June 2024

Natural Hazards and Earth System Sciences
Open Access
EGU
Discussions

Tsunami detection methods for Ocean-Bottom Pressure Gauges

Cesare Angeli[1], Alberto Armigliato[1], Martina Zanetti[1], Filippo Zaniboni[1], Fabrizio Romano[2], Hafize Başak Bayraktar[2], and Stefano Lorito[2]

[1]University of Bologna, Department of Physics and Astronomy "Augusto Righi" (DIFA), Bologna, Italy
[2]Istituto Nazionale di Geofisica e Vulcanologia (INGV), Rome, Italy

Correspondence: Cesare Angeli (cesare.angeli2@unibo.it)

Abstract. Real-time detection of tsunami waves is a fundamental part of tsunami early warning and alert systems. Several algorithms have been proposed in the literature for that. Three of them and a newly developed one, based on the Fast Iterative Filtering technique, are applied here to a large number of records from the DART monitoring network in the Pacific Ocean. The techniques are compared in terms of earthquake and tsunami event-detection capabilities and statistical properties of the detection curves. The classical Mofjeld's algorithm is very efficient in detecting seismic waves and tsunamis, but it does not always characterize the tsunami waveform correctly. Other techniques, based on Empirical Orthogonal Functions and cascade of filters respectively, show better results in wave characterization but they usually have larger residual than Mofjeld's. The FIF-based detection method shows promising results in terms of detection rates of tsunami events, filtering of seismic waves and characterization of wave amplitude and period. The technique is a good candidate for monitoring networks and in data assimilation applications for realtime tsunami forecasts.

1 Introduction

Tsunami early warning and alert systems operations are based on the rapid earthquake characterization in terms of magnitude and hypocenter after which alerts are typically given based on a decision matrix or on databases of pre-computed tsunami propagation scenarios; the forecast can be then confirmed, updated, or canceled based on additional earthquake information (e.g., focal mechanism, moment tensor, finite fault models) and sea level measurements (Duputel et al., 2011; Lomax and Michelini, 2013; Amato et al., 2021; Titov et al., 2005). The latter are crucial for the rapid characterization of tsunami waves, monitored from tsunami warning centres by means of coastal tide gauges and/or Ocean-Bottom Pressure Gauges (OBPG) (Rabinovich and Eblé, 2015).

Historically, the first tsunami recording instruments have been the coastal tide gauges, for which self-recording variants have been available since the 1830s (Matthäus, 1972). Thanks to these, wave records for a few very old events are available, such as the tsunami that followed the 1883 Krakatau eruption (Pelinovsky et al., 2005) and the one caused by the 1887 Ligurian earthquake (Eva and Rabinovich, 1997). However, tsunami detection was not the purpose of these first tide gauges, so the

https://doi.org/10.5194/nhess-2024-113
Preprint. Discussion started: 24 June 2024

Natural Hazards and Earth System Sciences
Open Access
EGU
Discussions

available records are still sparse. Thanks to recent technological advances which allow the adoption of sampling times in the order of seconds, tide gauges have become a fundamental source of data to analyse tsunamis, both for retrospective studies (Satake, 1987; Pires and Miranda, 2001; Romano et al., 2016) and real-time detection (Bressan et al., 2013; Lee et al., 2016). However, tide gauges suffer from a few drawbacks in the context of tsunami detection. First, they are able to detect a sea level anomaly only when it is already close to the coast, thus there might not be enough time to alert the local population at risk. Second, the tsunami evolution at coastal locations is deeply influenced by its nonlinear interaction with the local bathymetry and topography; indeed, the tide gauges are typically located in bays and harbours which have quite complex response spectra (Rabinovich, 1997; Aranguiz et al., 2019).

Conversely, these site-effects are negligible in case of measurements of tsunami waves in deep water environments using OBPG. By virtue of being located at the bottom of the ocean, these instruments only detect long waves signals, such as tsunamis and tides, filtering out naturally the most superficial oscillations; moreover, the open ocean tsunami evolution is less affected by complex interactions with coastal morphology and it is mostly a linear phenomenon. Thus, the signals from ocean-bottom measurements are a superposition of

1. tidal oscillations, dominated by diurnal and semidiurnal periods, which are the main contribution to the energy of the signal;
2. random oscillations in the same frequency range of tides, not accounted for by harmonic analysis;
3. tsunami waves;
4. changes in pressure due to displacement of the ocean bottom;

This last case is evident in the case of gauges subjected to seismic shaking, as for instruments located relatively close to the earthquake source zone, for which seismic and tsunami waves may not be well separated in the recordings, making the extraction of the tsunami wave quite challenging. Thus, techniques able to separate the two contributions are necessary for instruments located near the potential earthquake sources (Williamson and Newman, 2019). For detailed discussions on the nature of deep-ocean pressure measurements, we refer to the various literature reviews, such as Rabinovich (1997); Goring (2008); Mungov et al. (2013); Rabinovich and Eblé (2015).

The advancements in OBPG technology allowed the development of operational networks of tsunami detecting instruments, such as the Deep-ocean Assessment and Reporting of Tsunamis (DART) network (Li, 2022), composed of a variable in time number of OBPG operating around the Pacific, northeastern Indian and north Atlantic Oceans, which continuously transmits pressure data; the sampling frequency increases in case of an event, which can be triggered by an automatically detection or an external signal. The recorded pressure changes is converted in sea level variation and can be then incorporated into the tsunami forecast with different methods, such as real-time source inversion (Titov et al., 2003; Tang et al., 2009), data assimilation methods (Wang et al., 2019b; Maeda et al., 2015; Wang et al., 2017, 2019a; Heidarzadeh et al., 2019; Wang et al., 2021), or recently proposed Bayesian approaches (Selva et al., 2021b).

https://doi.org/10.5194/nhess-2024-113
Preprint. Discussion started: 24 June 2024

Natural Hazards and Earth System Sciences
Discussions

The purpose of this work is to test and compare real-time tsunami detection methods from the literature that have been applied to real data acquired by OBPGs. In particular, some techniques are chosen and then applied to past OBPG data *as if* it would happen in real-time. The first technique is the one proposed by Mofjeld (1997). Since every DART buoy has the algorithm implemented on board, the technique has a long story of applications and analysis of its properties (Beltrami, 2008, 2011; Chierici et al., 2017). It has to be noted that Fourth Generation DARTs (DART 4G) also include an additional algorithm which allows the automatic separation of seismic shaking and tsunami waves, exploiting the higher sampling rate (https://www.ndbc.noaa.gov/dart/dart.shtml). For that, 1 s sampling rate data are used (Moore, 2024). Since not enough information regarding DART 4G is publicly available, in this study, we do not deal with this algorithm, bur rather test the other algorithms on largely available DART data with sampling times of 15 s. Many of them are currently operational. It has also to be noted that even the on board sampling rate is higher, the ordinary transmission rate are lower, and the on board computing capability are generally limited, in both cases to limit the battery consumption. Thus, it is desirable to have a detection algorithms that work for relatively low sampling rates.

The other techniques presented and tested are the detiding through Empirical Orthogonal Functions (Tolkova, 2009, 2010) and Tsunami Detection Algorithm developed by Chierici et al. (2017). At last, a new technique, similar to the one developed by Wang et al. (2020), is presented. This new technique is based on the Fast Iterative Filtering (FIF) technique (Cicone, 2020; Cicone and Zhou, 2021) and the IMFogram time-frequency representation (Barbe et al., 2020; Cicone et al., 2024a).

The four techniques, which we will refer to as DART, EOF, TDA and FIF for brevity, are described in their basic mathematical structure in section 2. Applications are then shown in section 3, in order to study how the techniques behave on signal with and without tsunamis.

2 Algorithms for real-time tsunami detection

2.1 DART algorithm

DART gauges in the NOAA monitoring network are equipped with an automatic tsunami detection algorithm, described by Mofjeld (1997). The algorithm compares the pressure recorded at each instant with a prediction computed from the previously acquired data. If the absolute difference between these two values exceeds a given threshold, this is considered a detection of a sea level anomaly.

The predicted value is found by using using Newton's forward polynomial interpolation formula as

$$H_p(t') = \sum_{i=0}^{3} w_i \overline{H}(t - i\mathrm{d}t) \tag{1}$$

https://doi.org/10.5194/nhess-2024-113
Preprint. Discussion started: 24 June 2024

where t' is the prediction time set to $t+5.25\,\mathrm{s}$, $\overline{H}$ is the $10\,\mathrm{min}$ moving average of pressure data and $\mathrm{d}t = 60\,\mathrm{min}$. For the default parameters, it can be shown that

$$\begin{aligned} w_1 &= +1.16818457031250\\ w_2 &= -0.28197558593750\\ w_3 &= +0.14689746093750\\ w_4 &= -0.03310644531250 \end{aligned} \tag{2}$$

The technique is particularly suitable for on-board implementation, due to its very simple mathematical formulation, computational efficiency, and low requirements in terms of data needed for the prediction, since little more than the previous 3 hr of measurements are needed.

We note that the most recent point used for extrapolation is 5 min before current time. If a tsunami signal has a period longer than that, the averaging operation will not be able to remove it, so the extrapolation will be affected by the presence of the tsunami. The result is that residuals produced by Mofjeld's algorithm deviate in terms of amplitude and period from the tsunami waveform. The problem is addressed by Beltrami (2011), showing that a better agreement between the residual and the tsunami waveform may be obtained by adopting a longer prediction time. However, this results in a much smaller signal-to-noise ratio. The technique has no built-in method to filter out high frequency components, such as random noise and seismic waves.

2.2 EOF detiding

The use of Empirical Orthogonal Functions (EOFs) for detiding has been introduced by Tolkova (2009, 2010). The method is based on the application of Principal Component Analysis to a pressure record $\zeta(t)$ as follows:

1. extract from a long time series N segments of of M points length;
2. compute the covariance matrix

$$C_{ij} = \sum_{k=1}^{N} \left(\zeta(q_k + i - 1) - a_k\right)\left(\zeta(q_k + j - 1) - a_k\right) \tag{3}$$

   where q_k is the index where k-th fragment starts and a_k is the average of the k-th fragment;
3. compute the EOFs e_i as the eigenvectors of the matrix $C_{ij} + C_{M+1-i,M+1-j}$.

It is shown by Tolkova (2009) that the first few EOFs are sufficient to reconstruct the tidal component of the sea level signals. Furthermore, Tolkova (2010) shows that these bases have a universality property. In fact, if we compute the EOFs for data obtained in different locations, the residual produced by detiding a signal has the same amplitude whatever basis we use. For this reason, once we have data from a tsunameter in a basin, the technique may be applied to detide any signal from any other instrument within the same basin.

To apply the technique to real time tsunami detection, a 1 lunar day long basis is used. At each time step

https://doi.org/10.5194/nhess-2024-113
Preprint. Discussion started: 24 June 2024

1. the signal average is subtracted from the data;
2. tides are extracted by projecting the last acquired data onto the EOF basis;
3. a residual is computed by subtracting computed tides from the original signal;
4. the last residual point is compared with a given threshold;
5. once a new measurement is acquired, the computation is repeated on the new 1 lunar day time window that ends at that measurement.

The technique is computationally efficient, since computing the tides s by projection of a signal η can be done by a simple matrix-vector product as

$$s = EE^T\eta \tag{4}$$

where the matrix E has the EOF basis vector e_i as columns. It has also been shown that using 7 elements for the basis minimizes errors for the chosen signal length. In this work, the basis is obtained from the DART 46414 in the period between 06/06/2018 and 08/06/2022, since it presents no discontinuities or missing data. The obtained basis is shown in fig 1.

2.3 TDA

Tsunami Detection Algorithm (TDA), introduced by Chierici et al. (2017), has a modular structure, which includes tide prediction and signal filtering. Each time a new pressure measurement is acquired, tides are removed using a harmonic model (Pawlowicz et al., 2002) with precomputed coefficients. After that, a spike detection algorithm is used to eliminate isolated spikes. At last, the residual time history is band-pass filtered using a FIR filter. Since the TDA is designed to work in real-time, that is only utilizing previous data, a mirroring boundary condition is applied to the signal before filtering.

The TDA has been specifically developed to be as computationally efficient as possible and the processing at each time step requires only a few thousands floating point operations. Furthermore, the modularity makes it very easily adaptable to different operational conditions. On the other hand, requiring precomputed tidal coefficients puts a constraint on the applicability, since a relatively long time series, on the order of a few months, is needed at the position of the instrument. Thus, the technique as described by Chierici et al. (2017) cannot be applied to instruments which have been deployed too recently or have recorded jump discontinuities. Both of these events occur in the case of DART instruments, since they are periodically resurfaced for maintenance and downloading raw data, then deployed again in a different position. The case of jump discontinuities, due to resurfacing or other reasons, usually requires ad hoc processing, as in the case of very long (e.g., multiannual) trends (Mungov et al., 2013). Techniques to account for these occurrences in real-time need further investigation and are outside the scope of the present work. Whenever such a case is present for a signal in our datasets, TDA is not applied to it. An intermediate situation may occur, where enough data to compute a set of tidal coefficients are available, but not enough to remove tidal oscillations completely. In these cases, the residual produced by the technique may have amplitudes of several cm that may produce false detections even in absence of any anomaly. Local tidal ranges may also play a role, since areas with much larger tidal ranges

https://doi.org/10.5194/nhess-2024-113
Preprint. Discussion started: 24 June 2024

Natural Hazards and Earth System Sciences
Open Access
EGU
Discussions

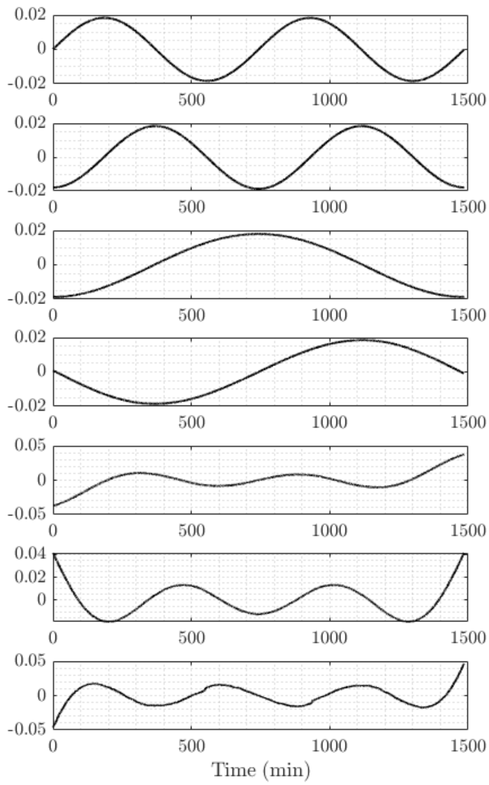

Figure 1. Empirical Orthogonal Functions computed for the DART 46414 (in the period 06/06/2018 - 08/06/2022) and used for EOF-based detection. The DART is located South East of Chirikov Island in the Alaskan Gulf.

are expected to have larger residuals. Given the modularity of TDA, different detiding techniques can be employed in place of the harmonic model presented (Consoli et al., 2014). However, this is outside the scope of the present analysis.

In this work, tidal coefficients are computed using UTide (Codiga, 2011) from at least 2 months of data ending few days before the time interval of interest in each case. For the harmonic filter, (Chierici et al., 2017) uses a 4000 points FIR pass band filter with a $[2\,\mathrm{min}, 120\,unitmin]$ or $[4\,\mathrm{min}, 120\,unitmin]$ period window. Here, we use the second window, since we are mainly interested in applications to tsunami of tectonic origin. Furthermore, filtering using this period band happens to filter out the frequencies which may be contaminated by infragravity waves (Mungov et al., 2013).

https://doi.org/10.5194/nhess-2024-113
Preprint. Discussion started: 24 June 2024

Natural Hazards and Earth System Sciences
Discussions

2.4 FIF-based tsunami detection

The FIF technique (Cicone, 2020) is a data-driven signal analysis technique for decomposing nonlinear and nonstationary signals into simple oscillatory components. The decomposition is additive, so that a signal $s(t)$ can be written as

$$s(t) = \sum_{k=1}^{N} I_k(t) + r(t) \tag{5}$$

where I_k are called Intrinsic Mode Functions (IMFs) and $r(t)$ is the residual. Each IMF satisfies the following properties:

1. the number of zero crossings and the number of relative extrema differ at maximum of one unity;

2. the envelopes of relative maxima and relative minima are symmetric with respect to zero.

A function with such properties can be regarded as a generalization of a Fourier mode $f(t) = A(t)\cos(\theta(t))$, where the amplitude $A(t)$ can vary with time and the phase $\theta(t)$ is allowed to be nonlinear (Huang et al., 1998).

The most common method to decompose a signal into IMFs is the Empirical Mode Decomposition (EMD), introduced by (Huang et al., 1998)). However, the FIF method has some properties that makes it preferable. In particular, it is more robust to noise (Cicone et al., 2016), it is not prone to mode mixing (Cicone et al., 2024b), and it generates no unwanted oscillations as defined by Cicone et al. (2022). The FIF shares some of these good properties with the Ensemble Empirical Mode Decomposition (EEMD, Wu and Huang (2009)), but for EEMD this comes with a severe increase in computational cost. On the contrary, FIF can be formulated using FFT (Cicone and Zhou, 2021) making it numerically efficient. To perform a time-frequency analysis of a signal, FIF is complemented by the IMFogram technique (Barbe et al., 2020; Cicone et al., 2024a). From the IMFogram, instantaneous amplitudes and frequencies are computed for each components from the envelope of the absolute value of extrema and the distribution of zero crossings, respectively.

The tsunami detection strategy we propose is as follows:

1. take the last 3 hours of acquired sea level data;

2. remove the long period trend by robust polynomial fit (Street et al., 1988);

3. decompose the residual using the FIF technique;

4. sum the IMFs with frequency content, computed with the IMFogram method, lies within a chosen frequency band;

5. compare the last point of the obtained signal with a chosen amplitude threshold;

6. repeat from step 1 once a new sea level measurement is acquired.

The reason for which the tidal trend is removed through polynomial fit lies in the ability of IMFs to capture components with variable frequency. Just after the arrival of a tsunami wave, as in the example in fig. 2, using FIF on raw data before detrending may not separate the tsunami wave from tides. For 3 hr long signals, polynomials of degree 3 seem to be the most appropriate.

https://doi.org/10.5194/nhess-2024-113
Preprint. Discussion started: 24 June 2024

Natural Hazards and Earth System Sciences
Discussions

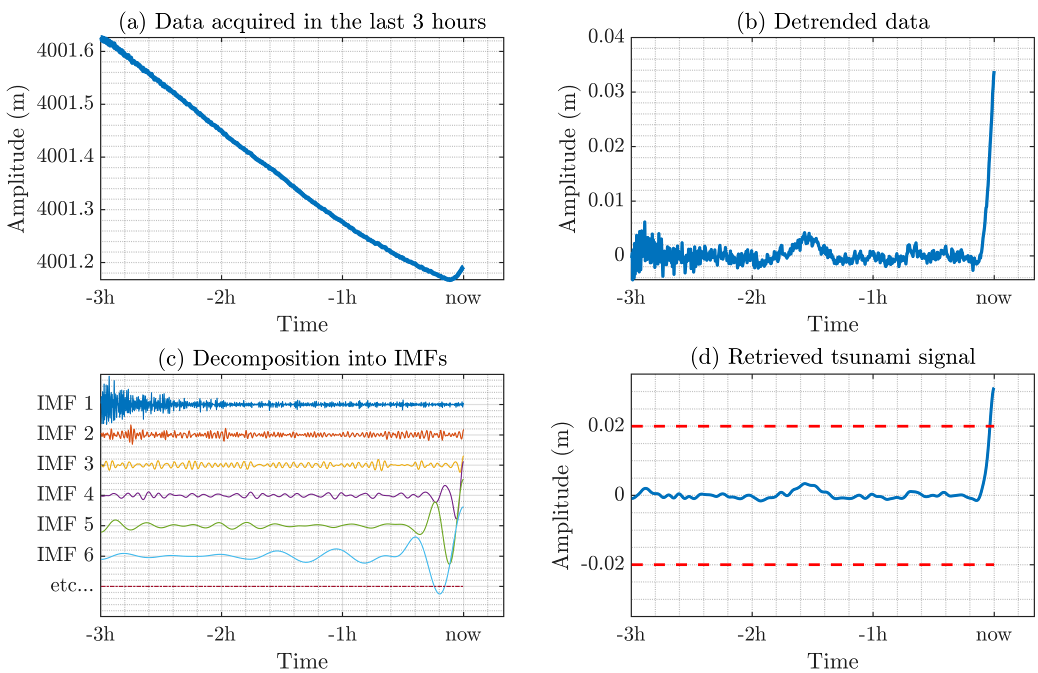

Figure 2. Example of FIF-based decomposition: (a) the last three hours of data are taken, (b) detrended through polynomial fitting, (c) decomposed using FIF and (d) the sum of components in the chosen frequency band are summed.

175 In terms of frequency band, in this work we retain components with periods between 4 min and 180 min. An example of the procedure for one time step is shown in fig. 2.

A similar detection technique based on data-driven signal decomposition was proposed by Wang et al. (2020). The FIF-based detection proposed here differs in two aspects. Firstly, they use the more computational expensive EEMD-based signal decomposition. Despite having two more steps, namely trend removal and frequency computation, than the technique by Wang
180 et al. (2020), the numerical efficiency of FIF makes our algorithm faster overall. Secondly, Wang et al. (2020) a-priori choose which components represent the tsunami, while we choose them based on the frequency content computed at each time step.

3 Performance comparison

To test the algorithms described in the previous sections, raw data from OBPG have been retrieved from the *Unassessed Ocean Bottom Pressure (highest available resolution)* catalog available on NOAA's website (https://www.ngdc.noaa.gov/thredds/
185 catalog/dart_bpr/rawdata/catalog.html).

All the techniques we consider here are amplitude based, that is they process the most recent available portion of data and then a detection is triggered based on the amplitude of the last point of the processed signal. To characterize the properties of

Natural Hazards and Earth System Sciences
Discussions

each technique, we analyse the time history made of these last points processed at each time step. We will refer to these time series as *detection curves*. The content of the detection curves is a superposition of residuals of the analysis and any component that is not filtered in the processing. However, the specific nature of these contributions differs between the techniques. For example, DART only removes long term trends, so detection curves contain oscillations from seismic and tsunami waves and random noise. For techniques that include detiding procedures, residuals in the frequency band of tides also contribute to the detection curves, which will then show coherent oscillations. The role of random instrumental noise is reduced wherever high-frequency filtering is used, e.g. for TDA and FIF, but not completely eliminated, since detection curves include only the last point of each analysis and are thus prone to errors from the boundary treatment. FIF detection curves may also be affected by errors in the polynomial fit. Anyway, the characteristics that we want from an ideal detection curve is to have an amplitude that increases in correspondence of the passage of a tsunami wave, while remaining below a given threshold anywhere else. Also, it is desirable to have them symmetric around zero. For example, in a detection curve with a negative bias, leading trough waves may be detected even if they have amplitude smaller than the detection threshold, while leading crest waves may not be detected even if taller than the threshold.

Each technique is applied to two different datasets. The first dataset consists of five time series, each being one month long, consisting only of tides and random noise, which we will refer to as *background signals*. In this way we are able to characterize the properties of the residual. The second includes day-long signals recorded at DART instrument during real tsunami events, to check if the techniques are able to detect tsunamis and if and when a detection is false or triggered by seismic shaking.

3.1 Background signal analysis

For the analysis of the background signal, we selected five time series of one month length, according to the following criteria:

1. no visible seismic or tsunami oscillations;
2. no instrumental spikes, holes or discontinuities;
3. part of a long deployment;

Furthermore, the different time series are taken from instruments installed in different areas around the Pacific Ocean, to avoid biases due to regional features.

Here, we illustrate the analysis by considering the signal chosen from DART 46414 (fig. 3) whose detection curves for each technique are shown in fig. 4. All detection curves show some residual oscillations, though of different amplitude and spectral content, as shown by the spectra in fig. 5. The EOF detection curve has peaks for periods around 24 hr, that is the residual from the main diurnal component, and 8 hr, which may be related to the fine structure of tidal oscillation, which is not captured by the algorithm Tolkova (2010). TDA has the main periods around 12 hr and 24 hr, showing that the main contribution to the residual is given by the difference between predicted and observed tides. DART and FIF detection curves also have a spectral peak around a period of 12 hr, but with a lower amplitude. Also, contrary to EOF, they have a mostly flat spectrum far from the semidiurnal frequency band.

https://doi.org/10.5194/nhess-2024-113
Preprint. Discussion started: 24 June 2024

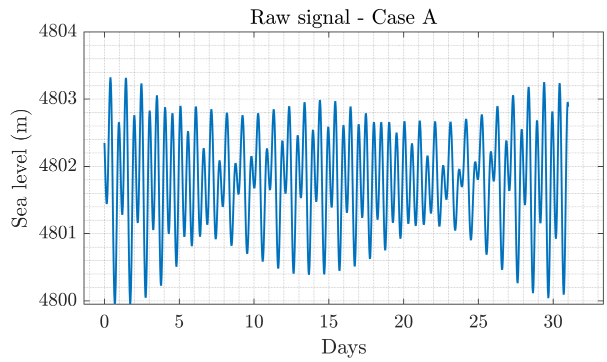

Figure 3. Raw data from DART 46414 for the month of August 2019.

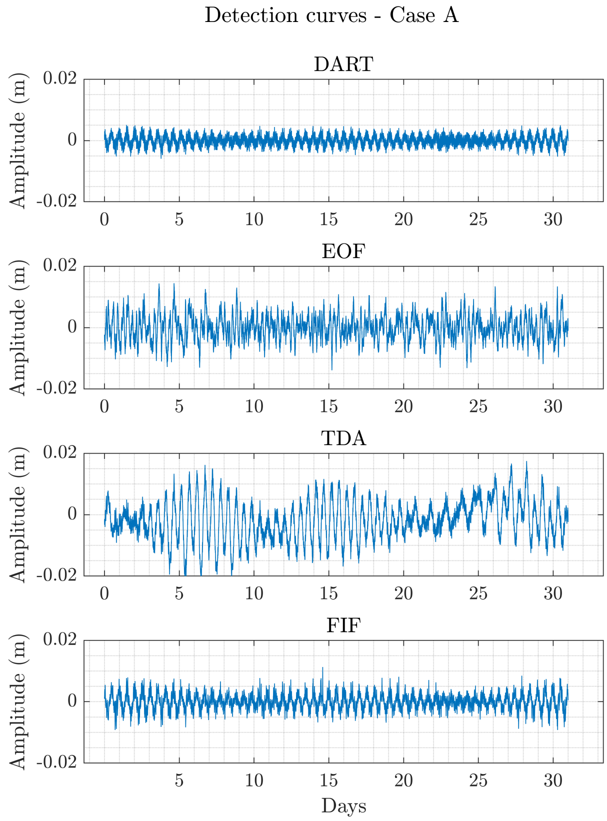

Figure 4. Detection curves for each detection technique for DART 46414, August 2019 (fig. 3).

https://doi.org/10.5194/nhess-2024-113
Preprint. Discussion started: 24 June 2024

Natural Hazards and Earth System Sciences
Open Access
Discussions

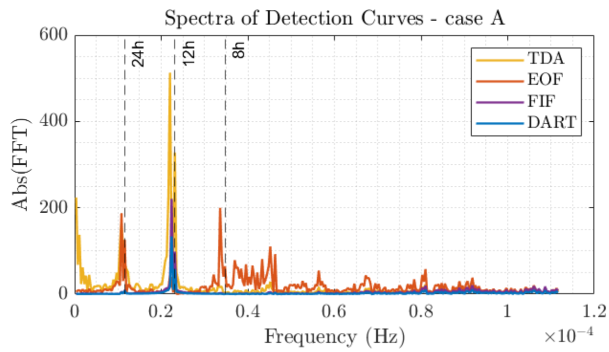

Figure 5. Detection curves for each detection curve in fig. 4, relative to data from DART 46414, August 2019 (fig. 3).

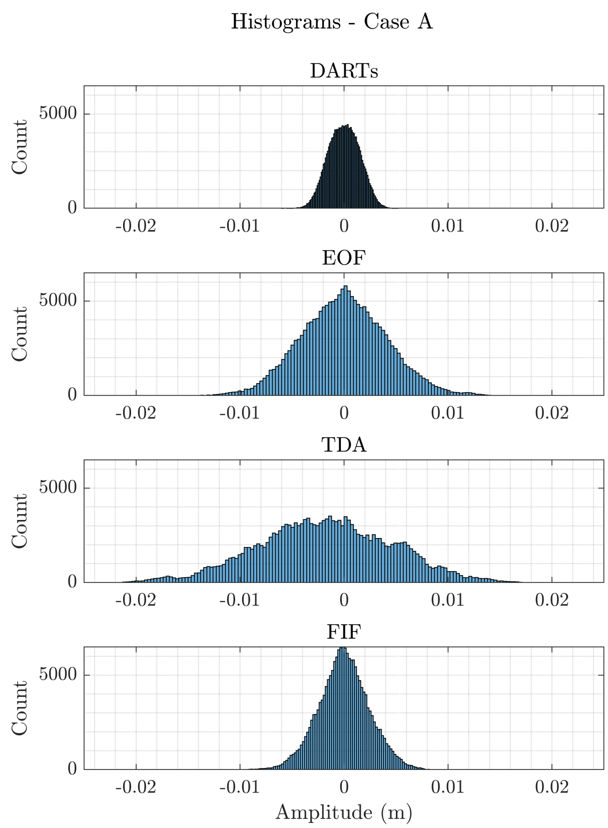

Figure 6. Histograms of each detection curve in fig. 4, relative to data from DART 46414, August 2019 (fig. 3).

https://doi.org/10.5194/nhess-2024-113
Preprint. Discussion started: 24 June 2024

Natural Hazards and Earth System Sciences
Open Access
EGU
Discussions

Table 1. Maximum peak-to-peak amplitude, indicated as A, of raw data and maximum variability range of detection curves for each technique in each background case. All quantities are expressed in cm.

Case	DART	Period	A	DART	EOF	TDA	FIF
A	46414	01/08/19 - 01/09/19	337.25	$[-0.59, 0.51]$	$[-1.39, 1.45]$	$[-2.16, 1.75]$	$[-0.92, 1.13]$
B	52402	01/06/16 - 01/07/16	82.04	$[-0.40, 0.42]$	$[-1.67, 1.85]$	$[-0.63, 1.25]$	$[-0.63, 0.71]$
C	32413	01/01/19 - 01/02/19	129.62	$[-0.54, 0.58]$	$[-1.72, 1.84]$	$[-1.30, 0.75]$	$[-0.74, 0.74]$
D	51407	15/04/22 - 15/04/22	88.70	$[-0.51, 0.54]$	$[-1.94, 1.93]$	$[-1.27, 0.82]$	$[-0.94, 0.97]$
E	21413	01/06/21 - 01/07/21	86.06	$[-0.44, 0.43]$	$[-1.71, 1.62]$	$[-0.69, 1.46]$	$[-0.64, 0.63]$

Table 2. Standard deviation expressed in cm for each technique in each background case.

Case	DART	Period	A	DART	EOF	TDA	FIF
A	46414	01/08/19 - 01/09/19	337.25	0.15	0.41	0.64	0.24
B	52402	01/06/16 - 01/07/16	82.04	0.10	0.56	0.27	0.15
C	32413	01/01/19 - 01/02/19	129.62	0.13	0.61	0.29	0.17
D	51407	15/04/22 - 15/04/22	88.70	0.13	0.63	0.30	0.20
E	21413	01/06/21 - 01/07/21	86.06	0.10	0.57	0.35	0.14

It is also interesting to look at the amplitude distribution of the prediction around zero. From the histograms in fig. 6, we can notice that the DART technique has the narrowest distribution, since it is able to remove the long-term trends entirely, with the only contribution to the detection curve being the random noise, as pointed out before. FIF has a very peaked distribution, indicating that the detection points checked at each time step do not deviate a lot from zero. On the other hand, EOF and TDA have a wider distribution, which shows that a larger number of values are further away from zero. For TDA, it can also be noticed that the histogram is not centered around zero, that is the points in the detection curve are distributed asymmetrically, due to the fact that the predicted tides are above the raw data.

The conclusions made for the case in fig. 3 can be generalized to the analysis of other background signals. The variability of the detection curves for all 5 cases is measured by their maximum range of variability and standard deviation, reported in tab. 1 and tab. 2, respectively, where the already analyzed example is case A. In each case, DART produces the narrowest distributions, both in terms of maximum variability, which is around $0.5\,\mathrm{cm}$ from zero, and in terms of standard deviation. FIF shows a larger variability for both metrics compared to DART, but lower than the other techniques, remaining within $1.2\,\mathrm{cm}$ from zero at each time. EOF is the technique with the largest standard deviations from the origin on average, followed by TDA, then FIF and DART, with the exception of case A, where TDA has larger standard deviation than EOF. This may be caused by the large tidal range in case A (see tab. 1), which results in less accurate tide prediction.

The asymmetric amplitude distribution of TDA is observed in all cases. Cases A, C, and D are negatively skewed, while cases B and E are positively skewed. On the contrary, the other techniques are approximately symmetrical in every case. For these 5 time series, the threshold of $3\,\mathrm{cm}$, commoly used in DART OBPGs (Mofjeld, 1997; Rabinovich and Eblé, 2015), produces no

https://doi.org/10.5194/nhess-2024-113
Preprint. Discussion started: 24 June 2024

Natural Hazards and Earth System Sciences
Discussions
Open Access

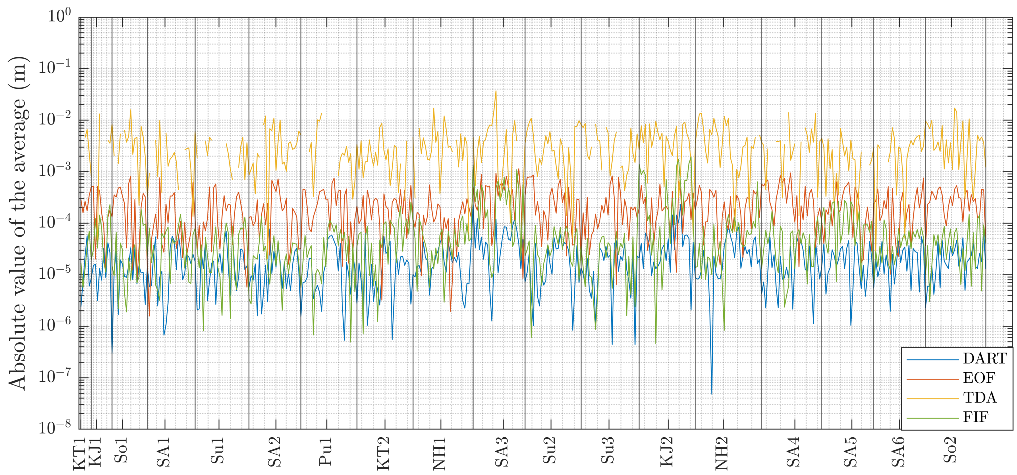

Figure 7. Absolute average value for each day-long detection curve in the dataset built on the catalog by Davies (2019).

false detection and seems to be a highly conservative choice. In fact, a 2 cm threshold would result in false detections only for TDA in case A. For DART and FIF, the threshold may be lowered to 1 cm and 1.5 cm respectively. Plots for cases B, C, D and E analogous to fig. 3 to 6 are reported in the Supplementary Materials.

3.2 Detection testing on past events

To test how the various algorithms compare in the detection of real events, a dataset based on the catalog by Davies (2019) has been built. The catalog includes 18 events that occurred around the Pacific Ocean between 2006 and 2016, generated by earthquakes of magnitude between 7.8 and 9.1. For each event, we extracted 24 hr long signals starting from the earthquake origin time from every OBPG active at origin time whose data are available on NOAA's website. It may happen that data may not be retrieved from some instruments. In these cases, only data transmitted in real-time by the instrument are available. For the DARTs concerned here, raw data's sampling time is 15 s, while it varies for transmitted data between 15 min for normal conditions, 15 s and 1 min for the 4 hr after a detection is triggered (Rabinovich and Eblé, 2015). For this reason, the cases where only transmitted data are available have been excluded. At last, we removed instrumental spikes and resampled by linear interpolation. The dataset obtained contains 437 signals of various nature: some of them consists of only background, while others also contain seismic and/or tsunami waves.

A first comparison between the different techniques can be made by computing the average and standard deviation of each detection curve. The comparison among absolute values of the averages (fig. 7) give results similar to the analysis of backgrounds in the previous section: DART usually produces the smallest residuals followed by FIF, EOF and at last TDA. TDA has a worse perfomance than before due to the variable availability of preceding data, as explained in section 2.3. Thus, TDA was not applicable to 55 signals whose deployment was too recent to compute tidal coefficients and it shows large

https://doi.org/10.5194/nhess-2024-113
Preprint. Discussion started: 24 June 2024

Natural Hazards and Earth System Sciences
Open Access
EGU
Discussions

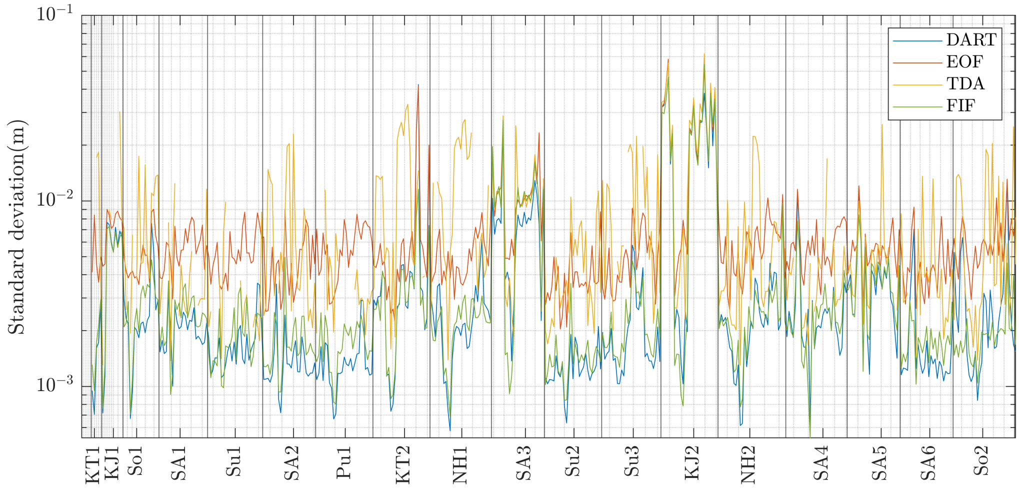

Figure 8. Standard deviation for each day-long detection curve in the dataset built on the catalog by Davies (2019).

residuals if the coefficients were computed from relatively short series. Standard deviations are correlated with the total area between the curve and horizontal axis, i.e. we expect the standard deviation to be proportional to amplitude of oscillations in a signal. Thus, the standard deviations of detection curves with low amplitude seismic and tsunami components behave similarly to curve averages, as shown in fig. 8. On the contrary, for signals with high amplitude seismic and/or tsunami components, the various techniques tend to provide similar results. This is evident for the case of the two Japan-Kurils and the Maule events (KJ1, KJ2 and SA3 respectively in the plot, see Davies (2019)).

To compare the four techniques, we now try to discriminate false detections and detections triggered by seismic shaking or the tsunami wave. We define for a given detection threshold T

- N: total number of signals in the dataset;
- n_F: number of signals with at least one false detection;
- n_E: number of signals with no false detection and at least one earthquake detection;
- n_T: number of signals with no false detection and at least one tsunami detection;
- Detection score 1: $\theta_1 = \dfrac{n_T - n_F}{N}$;
- Detection score 2: $\theta_2 = \dfrac{n_T - n_E - n_F}{N}$.

These parameters have been computed for each threshold from $T = 1.0\,\mathrm{cm}$ to $T = 4.0\,\mathrm{cm}$ with a step of 0.5 cm. We note that the process of attributing a detection to the seismic or tsunami wave trains has been carried out by visual inspection. To avoid possible biases, two strategies are employed. First, the attribution has been as conservative as possible, that is any

https://doi.org/10.5194/nhess-2024-113
Preprint. Discussion started: 24 June 2024

Natural Hazards and Earth System Sciences
Open Access
Discussions

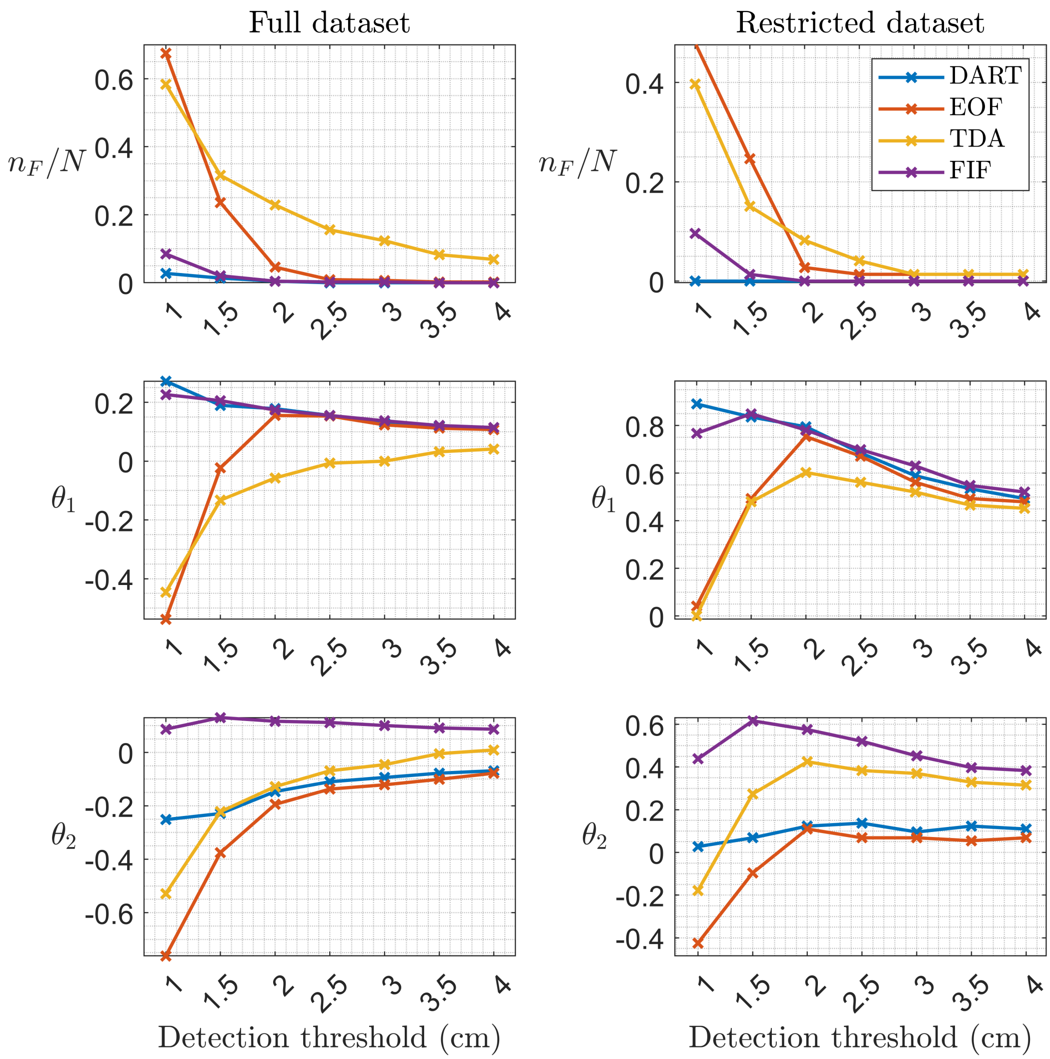

Figure 9. Normalised false detections n_F/N and detections scores θ_1, θ_2 for each detection technique for the full dataset (left column) and the restricted dataset of time series available in Davies (2019).

doubtful detection is considered a false detection. Second, we compared detection curves with post-processed waveforms made available by Davies (2019) to determine the nature of detections. The signals in the dataset for which these are available are 73. Furthermore, the analysis has been applied separately to the set of signals for which we have post-processed waveforms, which we refer to as *restricted dataset*, and to the full dataset.

The differences between techniques may be highlighted by comparing the number of false detections and the detection scores, reported in fig. 9 as functions of the detection threshold. The number of false detections decreases monotonically with the detection threshold, as we expect. DART and FIF both have zero false detections above a given threshold, namely 2.5 cm for the full dataset and 2.0 cm for the restricted one. On the contrary, EOF and TDA have false detections for each threshold among the ones considered. It is interesting to notice that both reach an asymptote in the restricted dataset for threshold bigger or equal to 3.0 cm. This is also the case in the full dataset for EOF, but not for TDA. The reason is that the full dataset contains a higher percentage of signals with larger tidal residual, which have an amplitude of several centimeters.

The behaviour is different in the case of the θ_1 and θ_2 scores. For θ_1, which can be interpreted as a measure of successful tsunami detections relative to the number of signals with false detections, we observe that DART gets always better with lower thresholds. On the other hand, for EOF θ_1 has a maximum for a threshold of 2.0 cm. This can be interpreted as the threhold that maximises the detection capabilities of EOF is θ_1 is assumed to be a good performance metric. TDA and FIF show a slightly different behaviour between the two dataset. FIF has an optimal threshold $T = 1.5\,\mathrm{cm}$ for the restricted dataset. TDA has the same optimum $T = 2.0\,\mathrm{cm}$ as EOF for the restricted dataset, while in the full dataset the presence of signals with large residual dominates as in the previous case.

θ_2 is similar to θ_1, with the added goal to minimise the number of earthquake detections. In the restricted dataset, DART and EOF perform worse than TDA and FIF, since the latter two filter out the high frequency content. Exactly as it happens for θ_1, EOF and TDA reach optimal score values at $T = 2.0\,\mathrm{cm}$ and FIF does at $T = 1.5\,\mathrm{cm}$. However, in the full dataset FIF is the only technique with an optimal threshold, again equal to 1.5 cm. For the other techniques, θ_2 increases monotonically with the detection threshold. While for TDA the reason is the same as before, DART's and EOF's performance is dominated by the larger amount of recorded seismic waves.

3.3 Waveform characterisation in FIF-based detection

According to Beltrami (2008), one of the desirable properties of a tsunami detection algorithm is the correct characterisation of the wave in terms of amplitude and period. While these properties have already been investigated for DART (Beltrami, 2011), EOF (Tolkova, 2009, 2010) and TDA (Chierici et al., 2017), they have yet to be established in case of FIF. In particular, we are interested in determining

1. the behaviour on signals where no earthquake or tsunami is present;
2. how seismic waves are filtered and the separation between Rayleigh waves and tsunami waves in the near field;
3. if we can determine the correct tsunami waveform from the detection algorithm.

Regarding point 1, detection curves generally behave as expected from the analysis of the background signal (see section 3.1), with amplitudes mostly within 1.0 cm and no strong residual oscillation.

For point 2, we already pointed out in section 3.2 that FIF filtering capabilities are well illustrated by the variation of θ_2 as a function of the detection threshold. However, even when the earthquake is detected, FIF allows to better separate seismic and tsunami waves. This is exemplified in fig. 10, showing the application of the techniques to DART 51425 record during the 29/09/2009 Samoa earthquake and tsunami. In this case, all four techniques would trigger a detection at the passage seismic

https://doi.org/10.5194/nhess-2024-113
Preprint. Discussion started: 24 June 2024

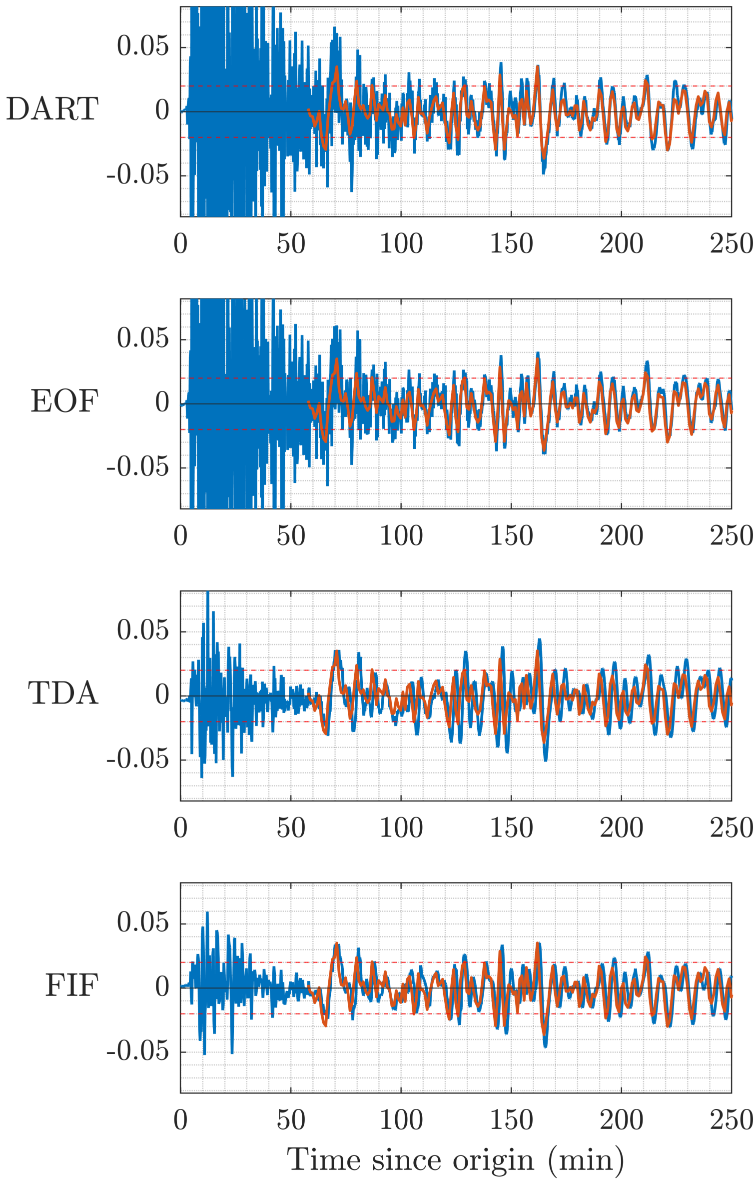

Figure 10. Comparison of detection curves (in blue) nand post-processed tsunami waveform (orange) for the 29/09/2009 Samoa tsunami as recorded in DART 51425. Dashed, horizontal, red lines are located at ±2 cm.

https://doi.org/10.5194/nhess-2024-113
Preprint. Discussion started: 24 June 2024

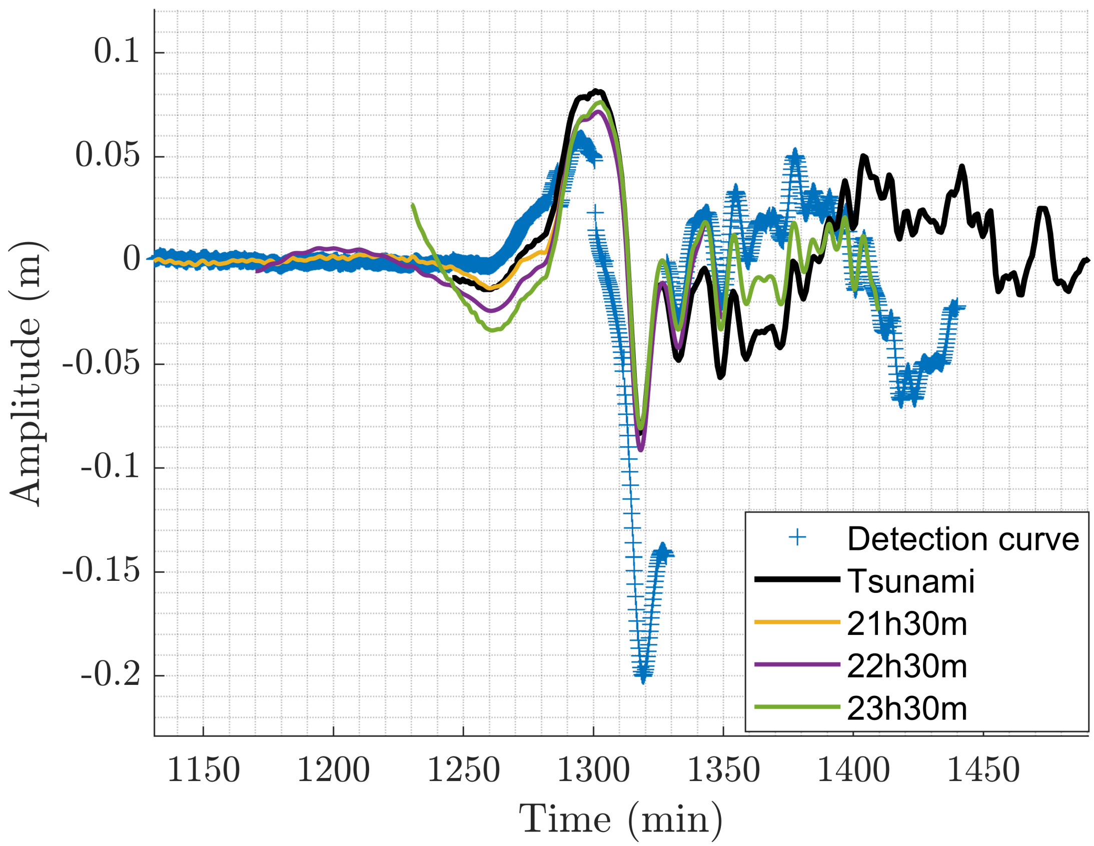

Figure 11. Example of the tsunami components (yellow, purple, and green curves) extracted during monitoring compared with the post-processed waveform (black) and the detection curve (blue crosses) obtained with the FIF-based technique. Time is measured from the earthquake origin time. Data from the record at DART 21413 for the 2010 Maule Tsunami.

waves, but the corresponding amplitude varies a lot between DART and EOF ($\sim$85 cm, not shown in figure) and TDA and FIF ($\sim$10cm). Furthermore, while for the first two the seismic wave train overlaps with the tsunami wave, for the last two there is a clear separation, allowing for a better estimation of the tsunami amplitude, which represents an important observable that is part of a tsunami alert statement.

In the analysis, we found a limited number of signals where FIF detection curves present jump discontinuities during the tsunami passage, in cases where the signal is very steep. Since the occurrence of these discontinuities only happen during a tsunami, they do not hinder in any way the detection capabilities of the technique. However, such cases may be problematic in data assimilation applications, where the full waveform is needed. In these cases, we can use the tsunami component produced by the decomposition (step 4 in the procedure described in section 2.4) at the time of assimilation.

https://doi.org/10.5194/nhess-2024-113
Preprint. Discussion started: 24 June 2024

Natural Hazards and Earth System Sciences
Discussions

As it is shown in fig. 11, the tsunami components extracted during monitoring at different times approximate the tsunami waveform much better then the detection curve by itself. However, the use of the full component extracted through FIF decomposition may be a heavy operation to perform in real time, since it would require transmission of a $3\,\mathrm{hr}$ long signal, that is a 720 element long vector, instead of a single number as needed for the detection curves. In instruments where power management is critical, such as DART buoys, this operation should be performed seldomly, e.g. once at a fixed time after detection, if precise data are needed, as is the case in data assimilation contexts (Wang et al., 2019b). At last, we also note that such large discontinuities in the detection curve are present in very few detection curves and that the example in fig. 11 is the most pathological.

4 Conclusions

Four tsunami real-time detection algorithms, one of which presented in this work for the first time, have been analyzed and compared. In particular, they have been tested against a large amount of real OBPG data from the DART network, both in the presence and in the absence of oscillations related to the earthquake and the tsunami. After determining the main properties of their residual on background signals, their detection capabilities have been tested and, wherever possible, optimal detection thresholds have been developed for different possible applications.

For detection applications only, Mofjeld's algorithm remains the most performing technique, both in terms of detection metrics and computational speed. However, the algorithm is not the most suitable to correctly characterize the tsunami waves, nor to filter out high frequency components (e.g. the seismic Rayleigh waves). The EOF and TDA techniques present variable behaviour. EOF is not able to reduce the tidal residual below $\sim 2\,\mathrm{cm}$, leading to incorrect characterization of low amplitude tsunami signals. TDA has a strong dependence on the precision of pre-computed tidal coefficients, resulting in a large number of detection curves with amplitude of several centimeters, too large for a precise detection of offshore travelling tsunamis. Investigating a combination of TDA with a different detiding technique may be the subject of future work.

The newly developed FIF-based detection method possibly shows the best compromise between detection and real-time characterisation. Optimal detection thresholds for the technique have been determined to be

1. $T = 2\,\mathrm{cm}$ for the goal of minimizing false detections;

2. $T = 1.5\,\mathrm{cm}$ for maximizing tsunami detection w.r.t. earthquake and false detections, based on two simple detection scores.

Furthermore, it is shown that the entire tsunami component over the three hour period reproduces accurately the tsunami waveform, allowing the characterization of wave amplitude and period even in the rare cases where the detection curves fail to do so.

Future work is planned for the application of the technique to the 4G DART buoys and non-OBPG data (e.g. coastal tide-gauges), and to tsunamis of nonseismic origin, for example for OBPGs which are planned at Stromboli to monitor volcano-induced tsunamis (Selva et al., 2021a). On the other hand, the technique is already fast enough to be applied in real-time, but an on-board implementation will require greater optimization to limit power consumption, especially in the case where the entire tsunami components has to be transmitted. Future work is then also planned for the numerical optimization of the technique by exploiting the recent installation of SMART cables (Howe et al., 2019) and also in view of the recent installations in the Ionian Sea of a dedicated instrumented cable to detect earthquakes and tsunamis (Marinaro et al., 2024), and of further DART-like OBPGs by CAT-INGV (Amato et al., 2021).

Code and data availability. All data used in the work are available in the *Unassessed Ocean Bottom Pressure (highest available resolution)* catalog available on NOAA's website (https://www.ngdc.noaa.gov/thredds/catalog/dart_bpr/rawdata/catalog.html). The computation of tidal coefficients has been carried out using UTide (Codiga, 2011), available at https://www.po.gso.uri.edu/~codiga/utide/utide.htm. For the FIF technique (Cicone, 2020) and the IMFogram algorithm (Barbe et al., 2020; Cicone et al., 2024a), we used the codes developed by the original developers of the techniques, available at https://github.com/Acicone/. Everything else, such as the FIR filter coefficients and the Empirical Orthogonal Functions, has been computed through native MATLAB functions.

Author contributions. Cesare Angeli: conceptualization, data curation, software, methodology,writing - original draft. Alberto Armigliato: supervision, methodology, writing - review and editing. Filippo Zaniboni: writing - review and editing. Martina Zanetti: software. Fabrizio Romano: methodology, writing - review and editing. Hafize Başak Byraktar: data curation. Stefano Lorito: supervision, methodology, writing - review and editing.

Competing interests. The contact author has declared that none of the authors has any competing interests.

Acknowledgements. The authors would like to Christopher Moore for the insightful discussions regarding DART buoys and the properties of tsunami detection algorithms. The work has been carried out as part of the collaboration "Accordo di collaborazione tra DIFA e INGV Roma con Rep. 51/2020 Prot. 803 del 08/05/2020".

Natural Hazards and Earth System Sciences
Open Access
Discussions

References

Amato, A., Avallone, A., Basili, R., Bernardi, F., Brizuela, B., Graziani, L., Herrero, A., Lorenzino, M. C., Lorito, S., Mele, F. M., et al.: From seismic monitoring to tsunami warning in the Mediterranean Sea, Seismological Research Letters, 92, 1796–1816, https://doi.org/10.1785/0220200437, 2021.

Aranguiz, R., Catalán, P., Cecioni, C., Bellotti, G., Henriquez, P., and González, J.: Tsunami resonance and spatial pattern of natural oscillation modes with multiple resonators, Journal of Geophysical Research: Oceans, 124, 7797–7816, https://doi.org/10.1029/2019JC015206, 2019.

Barbe, P., Cicone, A., Li, W. S., and Zhou, H.: Time-frequency representation of nonstationary signals: the IMFogram, arXiv preprint arXiv:2011.14209, https://doi.org/10.48550/arXiv.2011.14209, 2020.

Beltrami, G. M.: An ANN algorithm for automatic, real-time tsunami detection in deep-sea level measurements, Ocean Engineering, 35, 572–587, https://doi.org/10.1016/j.oceaneng.2007.11.009, 2008.

Beltrami, G. M.: Automatic, real-time detection and characterization of tsunamis in deep-sea level measurements, Ocean Engineering, 38, 1677–1685, https://doi.org/10.1016/j.oceaneng.2011.07.016, 2011.

Bressan, L., Zaniboni, F., and Tinti, S.: Calibration of a real-time tsunami detection algorithm for sites with no instrumental tsunami records: application to coastal tide-gauge stations in eastern Sicily, Italy, Natural Hazards and Earth System Sciences, 13, 3129–3144, https://doi.org/10.5194/nhess-13-3129-2013, 2013.

Chierici, F., Embriaco, D., and Pignagnoli, L.: A new real-time tsunami detection algorithm, Journal of Geophysical Research: Oceans, 122, 636–652, https://doi.org/10.1002/2016JC012170, 2017.

Cicone, A.: Iterative filtering as a direct method for the decomposition of nonstationary signals, Numerical Algorithms, 85, 811–827, https://doi.org/10.1007/s11075-019-00838-z, 2020.

Cicone, A. and Zhou, H.: Numerical analysis for iterative filtering with new efficient implementations based on FFT, Numerische Mathematik, 147, 1–28, https://doi.org/10.1007/s00211-020-01165-5, 2021.

Cicone, A., Liu, J., and Zhou, H.: Adaptive local iterative filtering for signal decomposition and instantaneous frequency analysis, Applied and Computational Harmonic Analysis, 41, 384–411, https://doi.org/10.1016/j.acha.2016.03.001, 2016.

Cicone, A., Li, W. S., and Zhou, H.: New theoretical insights in the decomposition and time-frequency representation of nonstationary signals: the IMFogram algorithm, arXiv preprint arXiv:2205.15702, https://doi.org/10.48550/arXiv.2205.15702, 2022.

Cicone, A., Li, W. S., and Zhou, H.: New theoretical insights in the decomposition and time-frequency representation of nonstationary signals: the imfogram algorithm, Applied and Computational Harmonic Analysis, 71, 101 634, 2024a.

Cicone, A., Serra-Capizzano, S., and Zhou, H.: One or two frequencies? the iterative filtering answers, Applied Mathematics and Computation, 462, 128 322, https://doi.org/10.1016/j.amc.2023.128322, 2024b.

Codiga, D. L.: Unified tidal analysis and prediction using the UTide Matlab functions, https://doi.org/10.13140/RG.2.1.3761.2008, 2011.

Consoli, S., Recupero, D. R., and Zavarella, V.: A survey on tidal analysis and forecasting methods for Tsunami detection, arXiv preprint arXiv:1403.0135, https://doi.org/10.48550/arXiv.1403.0135, 2014.

Davies, G.: Tsunami variability from uncalibrated stochastic earthquake models: tests against deep ocean observations 2006–2016, Geophysical Journal International, 218, 1939–1960, https://doi.org/10.1093/gji/ggz260, 2019.

Duputel, Z., Rivera, L., Kanamori, H., Hayes, G. P., Hirshorn, B., and Weinstein, S.: Real-time W phase inversion during the 2011 off the Pacific coast of Tohoku Earthquake, Earth, planets and space, 63, 535–539, https://doi.org/10.5047/eps.2011.05.032, 2011.

https://doi.org/10.5194/nhess-2024-113
Preprint. Discussion started: 24 June 2024

Natural Hazards and Earth System Sciences
Open Access
Discussions

Eva, C. and Rabinovich, A. B.: The February 23, 1887 tsunami recorded on the Ligurian coast, western Mediterranean, Geophysical Research Letters, 24, 2211–2214, https://doi.org/10.1029/97GL02110, 1997.

Goring, D.: Extracting long waves from tide-gauge records, Journal of waterway, port, coastal, and ocean engineering, 134, 306–312, https://doi.org/10.1061/(ASCE)0733-950X(2008)134:5(306), 2008.

Heidarzadeh, M., Wang, Y., Satake, K., and Mulia, I. E.: Potential deployment of offshore bottom pressure gauges and adoption of data assimilation for tsunami warning system in the western Mediterranean Sea, Geoscience Letters, 6, 1–12, https://doi.org/10.1186/s40562-019-0149-8, 2019.

Howe, B. M., Arbic, B. K., Aucan, J., Barnes, C. R., Bayliff, N., Becker, N., Butler, R., Doyle, L., Elipot, S., Johnson, G. C., et al.: SMART cables for observing the global ocean: science and implementation, Frontiers in Marine Science, 6, 424, https://doi.org/https://doi.org/10.3389/fmars.2019.00424, 2019.

Huang, N. E., Shen, Z., Long, S. R., Wu, M. C., Shih, H. H., Zheng, Q., Yen, N.-C., Tung, C. C., and Liu, H. H.: The empirical mode decomposition and the Hilbert spectrum for nonlinear and non-stationary time series analysis, Proceedings of the Royal Society of London. Series A: mathematical, physical and engineering sciences, 454, 903–995, https://doi.org/10.1098/rspa.1998.0193, 1998.

Lee, J.-W., Park, S.-C., Lee, D. K., and Lee, J. H.: Tsunami arrival time detection system applicable to discontinuous time series data with outliers, Natural Hazards and Earth System Sciences, 16, 2603–2622, https://doi.org/10.5194/nhess-16-2603-2016, 2016.

Li, H.: Deep-Ocean Assessment and Reporting of Tsunamis (DART) BUOY, pp. 306–314, Springer Nature Singapore, Singapore, ISBN 978-981-10-6946-8, https://doi.org/10.1007/978-981-10-6946-8_79, 2022.

Lomax, A. and Michelini, A.: Tsunami early warning within five minutes, Pure and Applied Geophysics, 170, 1385–1395, https://doi.org/10.1007/s00024-012-0512-6, 2013.

Maeda, T., Obara, K., Shinohara, M., Kanazawa, T., and Uehira, K.: Successive estimation of a tsunami wavefield without earthquake source data: A data assimilation approach toward real-time tsunami forecasting, Geophysical Research Letters, 42, 7923–7932, https://doi.org/10.1002/2015GL065588, 2015.

Marinaro, G., D'Amico, S., Embriaco, D., Giuntini, A., Simeone, F., O'Neill, J. Nicholson, B., Watkiss, N., and Restelli, F.: A 21 km SMART Cable for earthquakes and tsunami detection operating in the Ionian Sea, Tech. rep., Copernicus Meetings, https://doi.org/https://doi.org/10.5194/egusphere-egu24-16261, 2024.

Matthäus, W.: On the history of recording tide gauges, Proceedings of the Royal Society of Edinburgh, Section B: Biological Sciences, 73, 26–34, https://doi.org/10.1017/S0080455X00002083, 1972.

Mofjeld, H. O.: Tsunami Detection Algorithm, https://nctr.pmel.noaa.gov/tda_documentation.html, 1997.

Moore, C.: Personal communication, Private Communication, 2024.

Mungov, G., Eblé, M., and Bouchard, R.: DART® tsunameter retrospective and real-time data: A reflection on 10 years of processing in support of tsunami research and operations, Pure and Applied Geophysics, 170, 1369–1384, https://doi.org/10.1007/s00024-012-0477-5, 2013.

Pawlowicz, R., Beardsley, B., and Lentz, S.: Classical tidal harmonic analysis including error estimates in MATLAB using T_TIDE, Computers & Geosciences, 28, 929–937, https://doi.org/10.1016/S0098-3004(02)00013-4, 2002.

Pelinovsky, E., Choi, B., Stromkov, A., Didenkulova, I., and Kim, H.-S.: Analysis of tide-gauge records of the 1883 Krakatau tsunami, Tsunamis: Case studies and recent developments, pp. 57–77, https://doi.org/10.1007/1-4020-3331-1_4, 2005.

Pires, C. and Miranda, P. M.: Tsunami waveform inversion by adjoint methods, Journal of Geophysical Research: Oceans, 106, 19 773–19 796, https://doi.org/10.1029/2000JC000334, 2001.

https://doi.org/10.5194/nhess-2024-113
Preprint. Discussion started: 24 June 2024

Natural Hazards and Earth System Sciences
Open Access
EGU
Discussions

Rabinovich, A. B.: Spectral analysis of tsunami waves: Separation of source and topography effects, Journal of Geophysical Research: Oceans, 102, 12 663–12 676, https://doi.org/10.1029/97JC00479, 1997.

Rabinovich, A. B. and Eblé, M. C.: Deep-ocean measurements of tsunami waves, Pure and Applied Geophysics, 172, 3281–3312, https://doi.org/10.1007/s00024-015-1058-1, 2015.

Romano, F., Piatanesi, A., Lorito, S., Tolomei, C., Atzori, S., and Murphy, S.: Optimal time alignment of tide-gauge tsunami waveforms in nonlinear inversions: Application to the 2015 Illapel (Chile) earthquake, Geophysical Research Letters, 43, 11–226, https://doi.org/10.1002/2016GL071310, 2016.

Satake, K.: Inversion of tsunami waveforms for the estimation of a fault heterogeneity: Method and numerical experiments, Journal of Physics of the Earth, 35, 241–254, https://doi.org/10.4294/jpe1952.35.241, 1987.

Selva, J., Amato, A., Armigliato, A., Basili, R., Bernardi, F., Brizuela, B., Cerminara, M., de'Micheli Vitturi, M., Di Bucci, D., Di Manna, P., et al.: Tsunami risk management for crustal earthquakes and non-seismic sources in Italy, La Rivista del Nuovo Cimento, 44, 69–144, https://doi.org/https://doi.org/10.1007/s40766-021-00016-9, 2021a.

Selva, J., Lorito, S., Volpe, M., Romano, F., Tonini, R., Perfetti, P., Bernardi, F., Taroni, M., Scala, A., Babeyko, A., et al.: Probabilistic tsunami forecasting for early warning, Nature communications, 12, 5677, https://doi.org/10.1038/s41467-021-25815-w, 2021b.

Street, J. O., Carroll, R. J., and Ruppert, D.: A note on computing robust regression estimates via iteratively reweighted least squares, The American Statistician, 42, 152–154, https://doi.org/10.2307/2684491, 1988.

Tang, L., Titov, s., and Chamberlin, C.: Development, testing, and applications of site-specific tsunami inundation models for real-time forecasting, Journal of Geophysical Research: Oceans, 114, https://doi.org/10.1029/2009JC005476, 2009.

Titov, V. V., González, F. I., Mofjeld, H. O., and Newman, J. C.: Short-term inundation forecasting for tsunamis, Submarine Landslides and Tsunamis, pp. 277–284, https://doi.org/10.1007/978-94-010-0205-9_29, 2003.

Titov, V. V., Gonzalez, F. I., Bernard, E., Eble, M. C., Mofjeld, H. O., Newman, J. C., and Venturato, A. J.: Real-time tsunami forecasting: Challenges and solutions, Natural Hazards, 35, 35–41, https://doi.org/10.1007/s11069-004-2403-3, 2005.

Tolkova, E.: Principal component analysis of tsunami buoy record: Tide prediction and removal, Dynamics of atmospheres and oceans, 46, 62–82, https://doi.org/10.1016/j.dynatmoce.2008.03.001, 2009.

Tolkova, E.: EOF analysis of a time series with application to tsunami detection, Dynamics of Atmospheres and Oceans, 50, 35–54, https://doi.org/10.1016/j.dynatmoce.2009.09.001, 2010.

Wang, Y., Satake, K., Maeda, T., and Gusman, A. R.: Green's function-based tsunami data assimilation: A fast data assimilation approach toward tsunami early warning, Geophysical Research Letters, 44, 10–282, https://doi.org/10.1002/2017GL075307, 2017.

Wang, Y., Maeda, T., Satake, K., Heidarzadeh, M., Su, H., Sheehan, A., and Gusman, A.: Tsunami data assimilation without a dense observation network, Geophysical Research Letters, 46, 2045–2053, https://doi.org/10.1029/2018GL080930, 2019a.

Wang, Y., Satake, K., Cienfuegos, R., Quiroz, M., and Navarrete, P.: Far-field tsunami data assimilation for the 2015 Illapel earthquake, Geophysical Journal International, 219, 514–521, https://doi.org/10.1093/gji/ggz309, 2019b.

Wang, Y., Satake, K., Maeda, T., Shinohara, M., and Sakai, S.: A method of real-time tsunami detection using ensemble empirical mode decomposition, Seismological Research Letters, 91, 2851–2861, https://doi.org/10.1785/0220200115, 2020.

Wang, Y., Tsushima, H., Satake, K., and Navarrete, P.: Review on recent progress in near-field tsunami forecasting using offshore tsunami measurements: Source inversion and data assimilation, Pure and Applied Geophysics, 178, 5109–5128, https://doi.org/10.1007/s00024-021-02910-z, 2021.

https://doi.org/10.5194/nhess-2024-113
Preprint. Discussion started: 24 June 2024

Williamson, A. L. and Newman, A. V.: Suitability of open-ocean instrumentation for use in near-field tsunami early warning along seismically active subduction zones, Pure and Applied Geophysics, 176, 3247–3262, https://doi.org/10.1007/s00024-018-1898-6, 2019.

Wu, Z. and Huang, N. E.: Ensemble empirical mode decomposition: a noise-assisted data analysis method, Advances in adaptive data analysis, 1, 1–41, https://doi.org/10.1142/S1793536909000047, 2009.